CALICE Analysis Note CAN-040
April 17, 2013

Pion and proton showers in the CALICE scintillator-steel AHCAL: comparison of global observables

The CALICE Collaboration [1]

Abstract

The showers produced by positive hadrons in the CALICE scintillator-steel analogue hadronic calorimeter were studied using test beam data collected at CERN and FNAL for single particles with initial momentum from 10 to 80 GeV/c. The effective nuclear interaction length, calorimeter response and resolution, longitudinal and radial characteristics of proton and pion-induced showers were compared. The comparison was also performed with simulations using five physics lists from GEANT4 version 9.4.

[1]Corresponding author: Marina Chadeeva; marina@itep.ru

Contents

1 Introduction

Hadronic showers induced by different types of hadrons in a calorimeter are characterised by a relatively narrow core from electromagnetic component surrounded by an extended halo. The core is usually formed by electromagnetic cascades arising from π^0's decay. Such a complicated structure of hadronic showers results in significant fluctuations of their longitudinal and radial sizes as well as of calorimeter response to hadrons. There are some additional factors that strongly affect the hadron response and deteriorate the resolution for hadrons compared to that for electrons. The first factor is the so called *invisible* energy that is required to release nucleons from nuclei and is lost from being measured in the calorimeter. The second factor appears in non-compensating calorimeters and is due to significant event-by-event fluctuations of the electromagnetic fraction in hadronic showers.

Due to these additional factors, a response of calorimeter to hadrons is lower than to electrons and tends to be non-linear in non-compensating calorimeters [1, 2]. The energy dependence of the ratio of pion to electron response was measured for different calorimeters [3–5] and was found to not contradict the so called "power law behaviour" predicted by simulations [6].

Besides significant fluctuations of the hadronic response, differences in average response to different types of hadrons have been predicted in [6] and then observed experimentally [7] for pions and protons. The basis of such a prediction is the baryon conservation law resulting in a different dominating leading particle after each interaction - baryon in case of incoming baryon and meson including neutral pion in case of charged pion. It was demonstrated in [7] that the response for pions is $\sim$10% larger than that for protons in the energy range from 200 to 375 GeV. Such a behaviour was confirmed for lower energies (in the range from 20 to 180 GeV) by the recent studies performed for Fe-Scintillator ATLAS Tile calorimeter [8] where the response of pions was observed to be $\sim$4% higher than that of protons of the same initial energy.

In this study we analyse hadronic showers induced by positive pions and protons with initial energies from 10 to 80 GeV in the CALICE analogue scintillator-steel hadronic calorimeter (AHCAL). For both types of hadrons, the effective nuclear interaction length was estimated using an algorithm for identification of the longitudinal position of the first inelastic interaction. The calorimeter response and resolution as well as global observables such as mean longitudinal shower depth and mean shower radius are compared. The CALICE AHCAL response to protons is energy dependent and follows the phenomenological "power law", while pion response is linear in this energy range within $\pm$2% [9]. The estimated relative resolutions for pions and protons coincide within uncertainties. For all studied energies, proton showers were found to be on average $\sim$5% longer and $\sim$10% wider than pion showers.

In the second section the experimental setup and event selection procedures are described. The third section is dedicated to the comparison of extracted nuclear interaction lengths of pions and protons. The calorimeter response and resolution for hadrons are discussed

in the fourth section. And the fifth section contains estimates and comparisons of the global spatial parameters of hadronic showers.

2 Data and software

The analysis is based on the positive hadron data collected during CALICE test beams at CERN in 2007 and at FNAL in 2009. The energy reconstruction was performed using CALICE software version v04-02.

2.1 Experimental setup and calibration

The CALICE setup in CERN is described in detail in [9] and comprised a Si-W electromagnetic calorimeter (ECAL) [10], AHCAL [11] and tail catcher and muon tracker (TCMT) [12]. Positive pion beams in the momentum range from 30 to 80 GeV/c were delivered from CERN SPS H6 beam line. The data from threshold Čerenkov counter upstream calorimeter setup was used for offline discrimination between pions and protons on event-by-event basis.

The CALICE setup during the test beam campaign in FNAL is described in detail in [13]. In the current analysis, proton test beam data taken without electromagnetic calorimeter at initial momenta of 10 and 15 GeV/c were considered. The offline event-by-event separation of pions and protons was performed using both signals of differential Čerenkov counter placed upstream of the calorimeter setup.

The list of runs used for the current analysis is presented in Table 1. All runs analysed were taken at normal incidence of beam particle w.r.t. the calorimeter front plane. The sizes of the samples of π^+ and protons (the last two columns of Table 1) correspond to the samples of selected events with track in ECAL in case of CERN runs (see Section 2.2). The data samples extracted from runs taken at the same initial momentum were merged.

The visible signal in each calorimeter cell is obtained in units of MIP (minimum-ionising particle) as described in [11]. Only cells with a signal above 0.5 MIP were considered for further analysis and are called hits. The total deposited energy in units of GeV is calculated from the visible signal measured in different detector sections by multiplication with suitable electromagnetic calibration factors shown in Table 2. The Si-W ECAL comprises three sections with different sampling fractions and has a depth of approximately one nuclear interactions length λ_{I}. The AHCAL has 38 layers with equal sampling fraction and a depth of $\sim 5.3\lambda_{\mathrm{I}}$ (the electromagnetic calibration of AHCAL is described in [14]). The TCMT consists of two sections, the first section having the same sampling fraction as AHCAL; the absorber thickness of the second TCMT section is larger by a factor of 5 than in its first section [12]. Total depth of TCMT amounts up to $\sim 5.5\lambda_{\mathrm{I}}$. During the selection procedure, the conversion factors w were used to calculate the energy deposited

Table 1: List of used data runs and sample statistics.

Run number	Beam particle	Beam momentum GeV/c	Total number of events	Fraction of μ^+	Fraction of e^+	Fraction of multi-particle	Number of π^+	Number of protons
580060	proton	10	52045	2.8%	34.8%	15.5%	18533	4764
580063	proton	15	52445	3.5%	18.7%	16.0%	23034	8066
331298	π^+	30	191146	30.3%	n/e*	0.4%	33472	20490
331340	π^+	30	192061	30.0%	n/e	0.3%	33501	20909
331338	π^+	40	199435	4.6%	n/e	0.6%	66168	13210
331339	π^+	40	201035	4.5%	n/e	0.6%	66307	13500
331335	π^+	50	202068	4.4%	n/e	0.7%	67935	11905
331337	π^+	50	199799	4.3%	n/e	0.7%	67399	11704
331282	π^+	60	192636	3.6%	n/e	0.9%	61675	14491
331333	π^+	60	199699	3.9%	n/e	0.9%	64174	15039
331334	π^+	60	208954	3.8%	n/e	0.8%	66966	15760
331280	π^+	80	233225	3.2%	n/e	1.1%	63569	27599
331324	π^+	80	197042	2.7%	n/e	1.1%	54023	23574

* n/e - not estimated because of the requirement of a track in electromagnetic calorimeter for selected hadron events (see section 2.2 for details).

in the ECAL[2].

The conversion factor v from visible signal to deposited energy in the ECAL for non-showering hadrons was estimated using simulated muons in the ECAL and the measured muon response from test beam runs [15]. The factors v from the last column of Table 2 were used for selected events with minimum-ionising track in ECAL. The $\frac{e}{\pi}$ factor has to be considered in addition to calculate a reconstructed energy for hadrons. The same conversion coefficients and $\frac{e}{\pi}$ factor are applied to data and simulated samples.

2.2 Event selection

A hadron test beam is usually a mixture of different particles: hadrons, muons, electrons. The event selection comprises several steps and involves also the procedures of shower start and primary track finding. The shower start finding algorithm is described in detail in [16] and estimations of its quality using simulated samples are given in [17]. A primary track is identified assuming normal incidence w.r.t. the calorimeter front plane and using

[2]The electromagnetic calibration coefficients for ECAL are based on the CERN 2006 test beam data. For CERN 2007 data they might differ by several percent from indicated values. In the present analysis, the ECAL is effectively being used as a veto, because showers are required to start in the AHCAL, so a precise calibration of the ECAL at the electromagnetic scale is not essential.

Table 2: Conversion coefficients from visible signal to deposited energy, on the electromagnetic scale. In the last column, the coefficients for the conversion of visible signal to the energy loss of minimum ionising particles in ECAL are given, which are applied for events with track in ECAL.

Subdetector	Subsection number	Electromagnetic scale w, $\frac{GeV}{MIP}$	MIP scale v, $\frac{GeV}{MIP}$
ECAL	1	0.00376	0.002953
ECAL	2	0.00752	0.005906
ECAL	3	0.01128	0.008859
AHCAL		0.02364	-
TCMT	1	0.02364	-
TCMT	2	0.11820	-

a nearest neighbour criterion to select one hit per layer starting from the first front plane layer and up to the found shower start layer.

At the first step empty[3], multi-particle[4] and muon events are rejected. The detailed description of muon identification procedure as well as corresponding histograms can be found in [16]. This procedure is based on the comparison of the energy deposition in two sections: combined ECAL+AHCAL and TCMT. The constraint for deposition in combined section for FNAL runs without ECAL was scaled by a factor of 0.8 compared to the CERN setup configuration with ECAL in front of AHCAL. The highest muon contamination of ∼30% was observed for 30 GeV beams, while for other energies it did not exceed 5% (see Table 1). The contamination of selected pion samples with muons was estimated to be less than 0.5% for all energies.

As the analysed CERN runs (at 30 GeV/c and above) were taken with ECAL in front of AHCAL, the requirement of track in ECAL (shower start in AHCAL) is enough to reject possible positron admixture if any. For this reason, the positron contamination for the CERN runs was not estimated and is assumed to be negligible given this selection condition. Additional constraints are required for FNAL data taken without ECAL to reject positrons in the absence of electromagnetic calorimeter and without a possibility to use Čerenkov trigger that was set to separate pions from protons. The additional criterion for positron identification involves cuts on the mean shower radius R and on the longitudinal centre of gravity Z as electromagnetic showers are known to be more compact than hadronic ones. The corresponding parameters R and Z for a given event are defined in the following way:

[3]Any event that has less than 25 hits in both ECAL and AHCAL is considered as empty.

[4]The event is considered to be multi-particle if at least one of the following conditions is satisfied: (a) the deposited energy is higher than $E_{\text{beam}} + 2.4 \cdot \sqrt{E_{\text{beam}}}$ (E_{beam} in GeV); (b) more than 80 MIP or more than 13 hits are detected in the cells from the first five AHCAL layers which are more than 320 mm far from AHCAL centre; (c) parallel incoming tracks are identified before shower start.

$$R = \frac{\sum_{i=1}^{N_{\rm sh}} e_i \cdot r_i}{\sum_{i=1}^{N_{\rm sh}} e_i}, \tag{1}$$

where $N_{\rm sh}$ is the number of hits in AHCAL from shower start layer and beyond, e_i is the hit energy, $r_i = \sqrt{(x_i - x_0)^2 + (y_i - y_0)^2}$ is the distance from hit with coordinates (x_i,y_i) to shower axis with coordinates (x_0,y_0). The shower axis is defined using primary track coordinates in ECAL or event centre of gravity for the runs without ECAL.

$$Z = \frac{\sum_{i=1}^{N} e_i \cdot z_i}{\sum_{i=1}^{N} e_i}, \tag{2}$$

where N is the total number of hits in AHCAL and z_i is the distance from hit layer to the calorimeter front.

The joint distributions of R and Z are shown in Appendix A. The particle is considered to be a positron if the following condition is satisfied: $R < 37$ mm and $Z < 260$ mm. The efficiency of this criterion was estimated using positron runs taken in CERN with AHCAL only and is found to be ∼96% at 10 GeV and ∼97.5% at 15 GeV. The application of this cut to the negative pion samples extracted from CERN data (taken with ECAL in front) results in rejection of less than 0.8% of pions. The fraction of pions (protons) identified as positrons is also estimated from simulations with QGSP_BERT physics list and is ∼1.9% (∼0.8%) at 10 GeV and ∼1.6% (∼0.1%) at 15 GeV. The positron contamination for two FNAL runs estimated using this selection condition is shown in Table 1.

The samples from FNAL runs also need an additional cleaning from high admixture of multi-particle events that was not observed in CERN runs and cannot be excluded by means of the constraints mentioned above. For this purpose, an additional cut was set limiting total number of hits in the AHCAL to be ≤165 and ≤220 for 10 and 15 GeV, respectively. The application of these cuts to negative pion data samples extracted from the CERN runs results in rejection of less than 0.15% of events at 10 GeV and less than 0.07% of events at 15 GeV. The fraction of events rejected by applying these constraints to simulated hadron samples does not exceed 0.05% for pions and 0.01% for protons for all studied physics lists.

For further analysis (except for the study of nuclear interaction length), only events with shower start in the third, fourth and fifth AHCAL layers are used. The exclusion of events with shower start in the first and second AHCAL layer helps to significantly reduce the fraction of remaining positrons in the samples taken without ECAL. The exclusion of late showers (that start after fifth AHCAL layer) allows to minimise the leakage into TCMT and select hadronic showers which are mostly contained in the AHCAL.

The pion from proton separation in the test beam experiments fully relies on the Čerenkov counter efficiency whose impact on the proton sample purity is discussed in detail in Section 2.4 and Appendix B.

2.3 Global parameters of hadronic showers

The main parameters that characterise a calorimeter are the energy dependence of its response (linearity) and energy resolution. The understanding of leakage requires a study of longitudinal shower development and the implementation of PFA that involves a shower disentangling is in turn very sensitive to radial shower parameters. The following global parameters of hadronic showers were analysed and compared between pions and protons as well as between data and simulations:

- Reconstructed energy
- Energy resolution
- Mean longitudinal depth of hadronic shower
- Mean radial width of hadronic shower

2.3.1 Reconstructed energy and resolution

The reconstructed energy E_{event} of a hadron event with track in ECAL selected using the selection procedure described in Section 2.2 is calculated as follows:

$$E_{event} = \sum_{k=1}^{3} v_k \cdot M_k^{\mathrm{ECAL}} + \frac{e}{\pi}\left(w^{\mathrm{HCAL}} \cdot M^{\mathrm{HCAL}} + \sum_{k=1}^{2} w_k^{\mathrm{TCMT}} \cdot M_k^{\mathrm{TCMT}} \right), \qquad (3)$$

where $\frac{e}{\pi} = 1.19$ is the scaling coefficient to take into account a different response to electrons and hadrons in the non-compensating AHCAL (the coefficient was obtained for pions by averaging the ratio of beam energy to the total energy reconstructed at electromagnetic scale over the studied energy range); M_k^{ECAL}, M^{HCAL}, and M_k^{TCMT} are the sums of visible signals in the corresponding calorimeter subsections; weights v and w are taken from Table 2.

The reconstructed energy distributions were fitted with a Gaussian in the interval of ± 2 r.m.s. around the mean value. For some samples an interval ± 1.8 r.m.s. was used and $\chi^2/\mathrm{ndf} < 2$ was achieved for all fits. Hereinafter, the parameters of this Gaussian fit at a given beam energy are referred to as the mean reconstructed energy E_{reco} and resolution σ_{reco}, respectively.

2.3.2 Spatial parameters of hadronic showers

The longitudinal (along beam direction) centre of gravity of a hadronic shower can be calculated in two different ways: w.r.t. calorimeter front (see Eq. 2) and w.r.t. shower start as in the following equation:

$$Z0 = \frac{\sum_{i=1}^{N_{\mathrm{sh}}} e_i \cdot (z_i - z_{\mathrm{start}})}{\sum_{i=1}^{N_{\mathrm{sh}}} e_i}, \tag{4}$$

where N_{sh} is the number of hits in AHCAL from shower start layer and beyond, e_i is the hit energy, z_i is the distance from hit layer to the calorimeter front and z_{start} is the distance from shower start layer to the calorimeter front face. The observable Z calculated w.r.t. calorimeter front (see Eq. 2) is very helpful in event selection as discussed in Section 2.2. In contrast to Z, the value $Z0$ calculated w.r.t. shower start is independent on the distribution of shower start position and describes an intrinsic longitudinal shower development. This is important for comparison of different types of hadrons that have different nuclear interaction lengths.

In addition to $Z0$, the standard deviation σ_{Z0} of the energy weighted longitudinal hit position within a shower is calculated for each event using the following formula:

$$\sigma_{Z0} = \sqrt{\frac{\sum_{i=1}^{N_{\mathrm{sh}}} e_i \cdot (z_i - z_{\mathrm{start}} - Z0)^2}{\sum_{i=1}^{N_{\mathrm{sh}}} e_i}} \tag{5}$$

where N_{sh} is the number of hits in the AHCAL from the shower start layer and beyond, e_i is the hit energy, z_i is the distance from hit layer to the calorimeter front, z_{start} is the distance from shower start layer to the calorimeter front and $Z0$ is from Eq. 4.

The mean shower radius is calculated for each event using Eq. 1. It is an energy weighted sum of hit radial distances to the shower axis (in the plane perpendicular to the beam direction). The standard deviation σ_R that characterises the radial energy distribution within a shower is calculated for each event using the following formula:

$$\sigma_R = \sqrt{\frac{\sum_{i=1}^{N_{\mathrm{sh}}} e_i \cdot (r_i - R)^2}{\sum_{i=1}^{N_{\mathrm{sh}}} e_i}} \tag{6}$$

where N_{sh} is the number of hits in the AHCAL from the shower start layer and beyond, e_i is the hit energy, $r_i = \sqrt{(x_i - x_0)^2 + (y_i - y_0)^2}$ is the distance from hit with coordinates (x_i,y_i) to shower axis with coordinates (x_0,y_0) and R is from Eq. 1.

2.4 Systematic uncertainties

The uncertainty of beam momentum is taken into account using equation 5.1 from [14]. The following contributions to systematic uncertainty of the studied observables were analysed:

- δ_{MIP} from calibration and MIP to GeV conversion factor;

Table 3: Efficiencies of Čerenkov counter and purities of proton samples estimated for merged hadron samples.

Beam momentum GeV/c	Čerenkov counter efficiency ϵ_{muon}	Purity of proton sample η	
		all hadron events	start in AHCAL
10	0.91 ± 0.03	0.64 ± 0.16	0.66 ± 0.15
15	0.91 ± 0.03	0.71 ± 0.11	0.72 ± 0.10
30	0.97 ± 0.004	0.95 ± 0.01	0.95 ± 0.01
40	0.96 ± 0.01	0.84 ± 0.05	0.81 ± 0.06
50	0.96 ± 0.01	0.79 ± 0.06	0.75 ± 0.07
60	0.97 ± 0.01	0.89 ± 0.04	0.86 ± 0.04
80	0.90 ± 0.01	0.78 ± 0.03	0.74 ± 0.03

- δ_{e^+} from the uncertainty in the positron contamination in runs without ECAL;
- δ_η from the uncertainty in the pion contamination of proton samples due to inefficiency of the Čerenkov counter.

The calibration uncertainty δ_{MIP} contributes to the uncertainty of reconstructed energy and is shown in Table 4 in Appendix B. The systematic uncertainties of the calibration procedure were analysed in detail in the study of the AHCAL electromagnetic response [14]. The conversion coefficient from MIP to GeV for the AHCAL (see Table 2) was obtained from electron and positron runs with an accuracy of 0.9% [14], which takes into account a wide range of different systematic contributions studied in the electromagnetic analysis [9].

The procedure for estimation of the contributions δ_{e^+} and δ_η is discussed in detail in Appendix B. The purity of proton samples from pions depends on the efficiency of the Čerenkov counter used. The description of the procedure for estimation of the Čerenkov counter efficiency using muons ϵ_{muon} and proton sample purity η can be found in Appendix B. The estimated efficiencies and purities of proton samples for each beam energy are shown in Table 3. As the pressure in gaseous Čerenkov detector used was set well below proton threshold, we assume here that the probability of proton contamination in pion samples is negligible.

Due to positron contamination the mean reconstructed energy is overestimated while mean shower depth and width are underestimated. The admixture of pions in proton samples results in overestimation of proton nuclear interaction length and reconstructed energy and in underestimation of the longitudinal and radial sizes of proton showers. In this study, no correction for impurities is made for observed mean values, the corresponding biases are introduced as asymmetric systematic uncertainties instead.

The same algorithm of shower start finding is applied to both data and simulated samples and the systematic uncertainty due to shower start finding algorithm is assumed to be

canceled. This suggestion is supported by the fact that the estimates of nuclear interaction length, which are based on the algorithm used, are in good agreement between data and simulations (see Section 3).

The obtained estimates of spatial observables are still affected by leakage due to restricted AHCAL depth ($5.3\lambda_{\mathrm{I}}$) in spite of the applied selection by shower start. The shift due to leakage effect is negligible below 20 GeV and does not exceed several percent at 80 GeV. The main impact of the leakage is on the estimates of standard deviations. It should be noted that this shift does not affect the comparison of data and simulations.

2.5 Monte Carlo models

The simulations were done using the software packages Mokka v07_07p04 and GEANT4 version 9.4 patch 3 accompanied by the digitisation procedure from calice_soft v04-05 (with the conversion coefficient 816 keV/MIP and light crosstalk 0.1 for the AHCAL).

Five physics lists were studied: QGSP_BERT, QBBC, CHIPS, FTFP_BERT, and FTF_BIC. The detailed description of the involved models can be found in [13, 18].

3 Nuclear interaction length

The developed procedure of shower start identification allows to estimate the effective nuclear interaction length for a given calorimeter structure. The estimates for negative pions which were obtained using previous version of start finding algorithm are discussed in detail in [17]. In the current study, an updated algorithm with energy dependent criteria was applied to positive hadron data and simulated samples [16]. Typical distributions of the found shower start position are shown in Fig. 1 for data and QGSP_BERT physics list. The very good exponential behaviour ($\chi^2/\mathrm{ndf} < 1$ for fit) is observed for these distributions for all studied energies assuming the uncertainty of the algorithm to be approximately ± 1 AHCAL layer ($\approx$32 mm). Two first layers with large uncertainty of shower start finding algorithm as well as several last layers were excluded from the fit and the fit interval is from 65 mm to 900 mm for all samples.

The analysed pion samples contain negligible admixture of protons and the corresponding distribution $f(z)$ of shower start position z can be fitted with one exponential function:

$$f(z) = A \cdot \exp\left(-\frac{z}{\lambda_\pi}\right), \tag{7}$$

where A is a normalisation factor and λ_π is the estimated nuclear interaction length.

Fig. 2a shows the energy dependence of the nuclear interaction length for pions λ_π extracted from the fit with the function (7) to both simulated and data samples. The

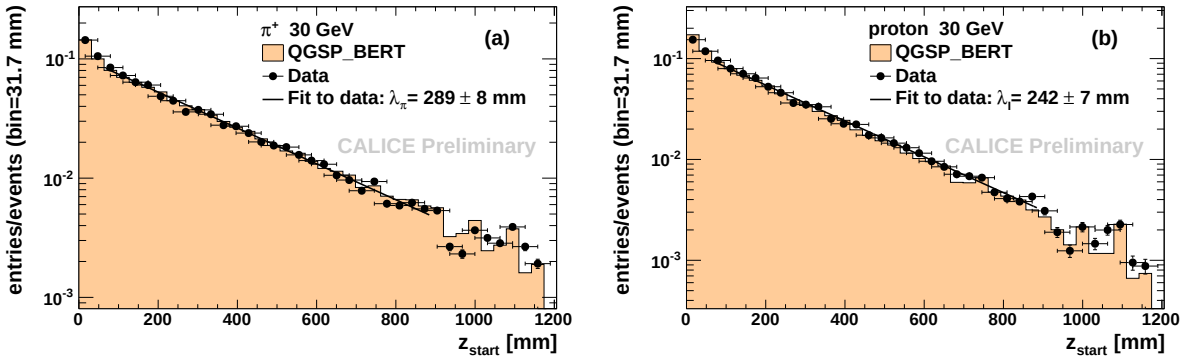

Figure 1: Distributions of the found shower start position in the AHCAL for data (black circles) and QGSP_BERT (filled histogram) for 30 GeV hadrons: (a) pions and (b) protons. The estimated nuclear interaction lengths obtained from the fit to data are shown in the legend. See text about fit details.

systematic uncertainties for data due to positron contamination are shown with grey band. They were estimated by varying the fit range and are found to be 2.6% at 10 GeV and <1% at 15 GeV. As follows from Fig. 2a, the estimated values of λ_π extracted from the found shower start for data and simulations are in good agreement between each other (except for QBBC) and agree with the estimation of the effective nuclear interaction length $\lambda_\pi^{\text{eff}} = 282$ mm for the CALICE analogue scintillator steel hadronic calorimeter obtained from PDG data [11, 19].

The studied proton data samples contain noticeable pion admixture that varies from 5% to 35%. The distribution of shower start position z for the sample that is a mixture of hadrons with different inelastic cross sections can be considered as a sum of two independent contributions:

$$f_{\text{mix}}(z) = A \cdot \left(\eta \cdot \exp\left(-\frac{z}{\lambda_{\text{I}}}\right) + (1-\eta) \cdot \exp\left(-\frac{z}{\lambda_\pi}\right) \cdot \frac{\lambda_{\text{I}}}{\lambda_\pi} \right), \tag{8}$$

where the normalisation factor A and the nuclear interaction length for protons λ_{I} are estimated variables, while the purity of proton sample η and the nuclear interaction length for pions λ_π are taken as previously determined and known parameters. The purity η (see Table 3) is estimated as described in Appendix B. The value of λ_π is extracted from the fit to the corresponding pion sample.

To estimate the systematic uncertainty due to errors of λ_π and purity, the following procedure was used. The set of parameter values was generated using Gaussian distributions with the sigma corresponding to the uncertainty of a given parameter and the generated values were used in the fit to proton data. The r.m.s. of the obtained distribution of λ_{I} is taken as a systematic uncertainty. The contributions from both parameters are summed up in quadrature and shown with grey band in Fig. 2b.

Fig. 2b shows the energy dependence of λ_{I} extracted from the fit with the function (8) to

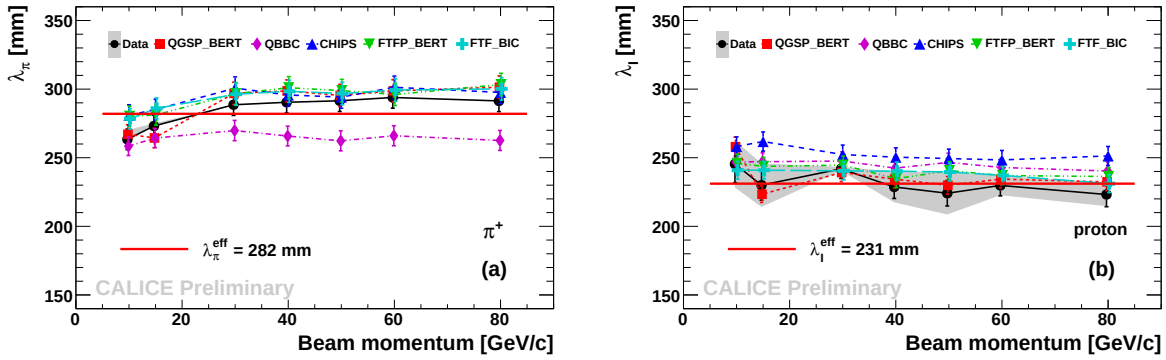

Figure 2: Nuclear interaction length λ_π for pions (a) and λ_I for protons (b) in the CALICE AHCAL versus beam momentum extracted for found shower start from data samples (black circles) and simulated samples using different GEANT4 physics lists. The red solid line corresponds to the effective nuclear interaction length calculated from PDG data for (a) pions $\lambda_\pi^{\mathrm{eff}}$ and (b) protons $\lambda_\mathrm{I}^{\mathrm{eff}}$. Systematic uncertainties for data are shown with grey band.

both data and simulated proton samples. A good agreement between data and simulations is observed. The obtained estimates of λ_I also agree with the estimate $\lambda_\mathrm{I}^{\mathrm{eff}} = 231$ mm obtained for the AHCAL structure using PDG data [19, 20]. The CHIPS physics list demonstrates a bigger disagreement ($\sim$8%) than other four physics lists studied here.

4 Calorimeter response and resolution

The AHCAL response for charged pions as well as some global parameters of charged pion showers have been discussed in detail in [9,17]. In test beam data, the calorimeter response for pions was observed to be linear within $\pm 2\%$ in the energy range 10-80 GeV and the fractional resolution for pions can be well described by the following three-component function:

$$\frac{\sigma}{E} = \frac{a}{\sqrt{E}} \oplus b \oplus \frac{c}{E}, \tag{9}$$

where E is in GeV, and $a = 0.58$ GeV$^{\frac{1}{2}}$, $b = 0.016$ and $c = 0.18$ GeV are stochastic, constant and noise contributions, respectively [9].

The current study is mostly focused on the comparison between pions and protons.

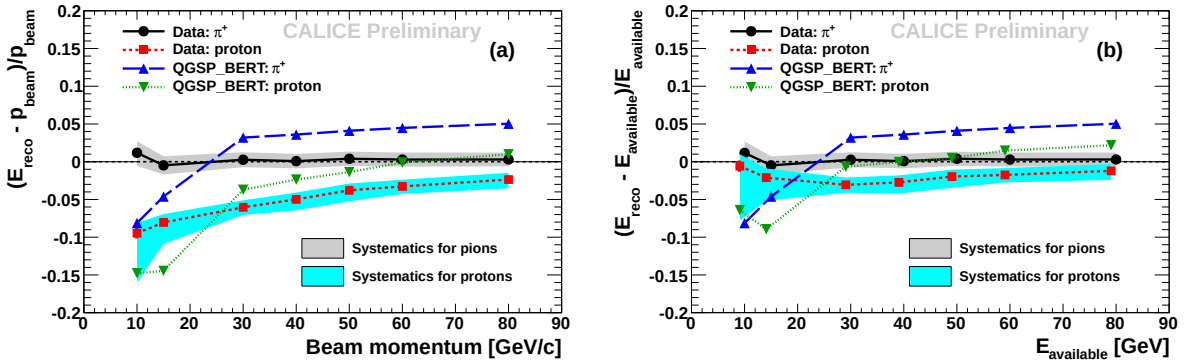

Figure 3: Relative residuals of reconstructed energy E_{reco} to (a) beam momentum and (b) available energy for data (black circles for pions and red squares for protons) and QGSP_BERT physics list (blue triangles for pions and green down triangles for protons). Systematic uncertainties for data are shown with grey band for pions and cyan band for protons.

4.1 AHCAL response for positive hadrons

The calorimeter response for protons was predicted and observed to be lower than that for pions [6–8]. The difference increases with decreasing initial particle energy and can be largely explained by the baryon conservation law that results in lower probability to produce leading baryon in pion interaction with nucleus. The so called "available energy" is introduced (i.e. available to be measured in the calorimeter) which corresponds to the total particle energy in case of mesons and to the kinetic energy of a particle in case of baryons:

$$E^{\mathrm{proton}}_{\mathrm{available}} = \sqrt{p^2_{\mathrm{beam}} + m^2_{\mathrm{proton}}} - m_{\mathrm{proton}}, \tag{10}$$

where p_{beam} is a beam momentum and m_{proton} is the proton rest mass.

Figure 3 shows the relative residuals both to beam momentum (a) and to available energy (b) for data and QGSP_BERT physics list for positive pions and protons in the energy range from 10 to 80 GeV. If the available energy is considered, the difference between positive pion and proton response remains at the level of ∼4%, in agreement with the difference observed in [8] for Sc-Fe Tile ATLAS calorimeter. The FTF_BIC physics list (Fig. 4) shows a similar behaviour and gives better predictions of response for pions than QGSP_BERT and very good prediction for protons above 20 GeV. The CHIPS physics list is in good coincidence with data below 20 GeV for both pions and protons. Additional illustrations for QBBC, CHIPS and FTFP_BERT physics lists can be found in Appendix C.

The so called $\frac{\mathrm{p}}{\pi}$ ratio describes the relative calorimeter response to pions and protons of the same initial energy ($\frac{\mathrm{p}}{\pi} = \frac{E^{\mathrm{p}}_{\mathrm{reco}}}{E^{\pi}_{\mathrm{reco}}}$) and is shown in Fig. 5 for data and different physics lists. As shown by Fig. 5a, the predictions of $\frac{\mathrm{p}}{\pi}$ by QGSP_BERT, QBBC and CHIPS coincide with data within systematic uncertainties because both pion and proton response

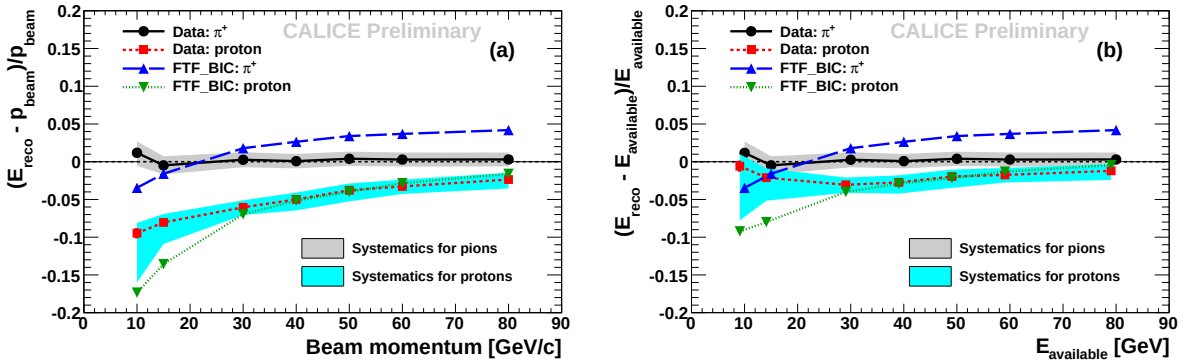

Figure 4: Relative residuals of reconstructed energy E_{reco} to (a) beam momentum and (b) available energy for data (black circles for pions and red squares for protons) and FTF_BIC physics list (blue triangles for pions and green down triangles for protons). Systematic uncertainties for data are shown with grey band for pions and cyan band for protons.

is simultaneously underestimated and overestimated by these physics lists. Fritiof-based physics lists (FTFP_BERT and FTF_BIC in Fig. 5b) underestimate this value due to overestimation of pion response while the proton response is quite well reproduced.

4.2 AHCAL energy resolution

The fractional energy resolution for protons in data is in good agreement with that for pions as demonstrated by Fig. 6. The earlier performed fit with Eq. 9 to pion data [9] is shown with black solid curve. The QGSP_BERT physics list gives a very good prediction of fractional resolution for both pions and protons (the best from all physics lists). The FTF_BIC physics list overestimates the fractional resolution slightly for protons and significantly for pions at 30 GeV/c and above.

The additional illustrations for QBBC, CHIPS and FTFP_BERT physics lists can be found in Appendix C.

5 Longitudinal and radial parameters of hadronic showers

One of the important factors that impact jet energy resolution is a shower containment in the calorimeter, which is tightly related to the longitudinal leakage. At the same time, the application of the PFA approach involves a procedure of disentangling of hadronic showers induced by charged and neutral hadrons in the calorimeter. In this context it is important to understand the radial size of hadronic shower that is a key factor for disentangling efficiency. The mean longitudinal and radial characteristics of hadronic showers are calculated on an event-by-event basis as well as the corresponding standard

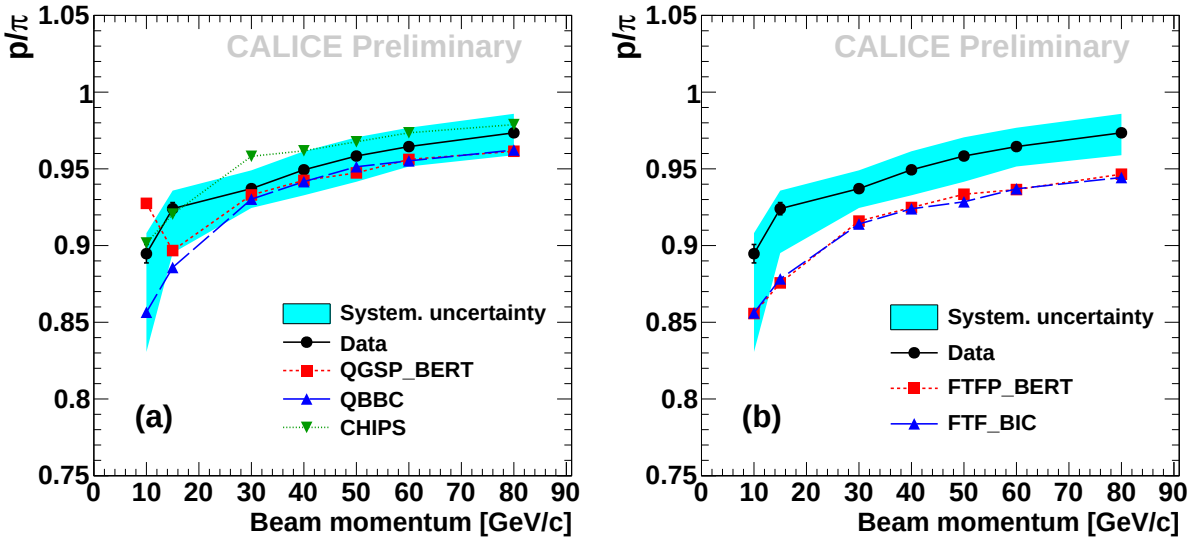

Figure 5: $\frac{p}{\pi}$ ratio versus beam momentum for data (black circles) and (a) QGSP_BERT, QBBC and CHIPS physics lists and (b) FTFP_BERT and FTF_BIC physics lists. Cyan bands show systematic uncertainties for data.

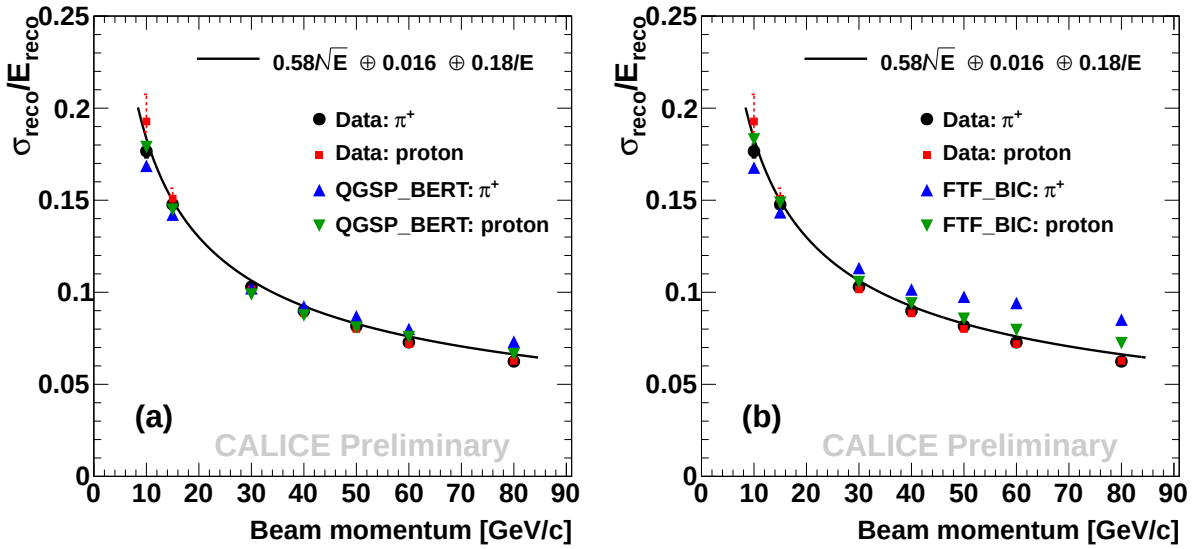

Figure 6: Fractional energy resolution versus beam momentum for data (black circles for pions and red squares for protons) and simulations (blue triangles for pions and green down triangles for protons) using (a) QGSP_BERT and (b) FTF_BIC physics lists.

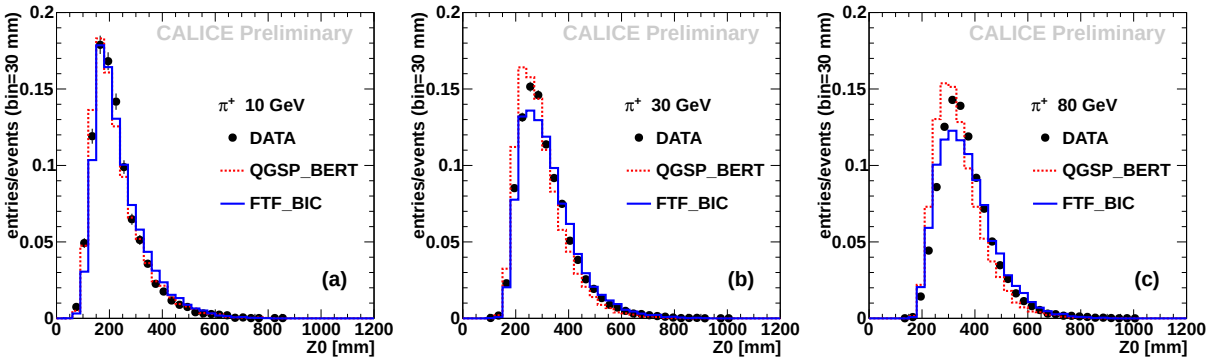

Figure 7: Distributions of the longitudinal centre of gravity for pion-induced showers at initial momentum (a) 10 GeV/c, (b) 30 GeV/c and (c) 80 GeV/c for data (black circles) and QGSP_BERT (red dashed line) and FTF_BIC (blue solid line) physics lists.

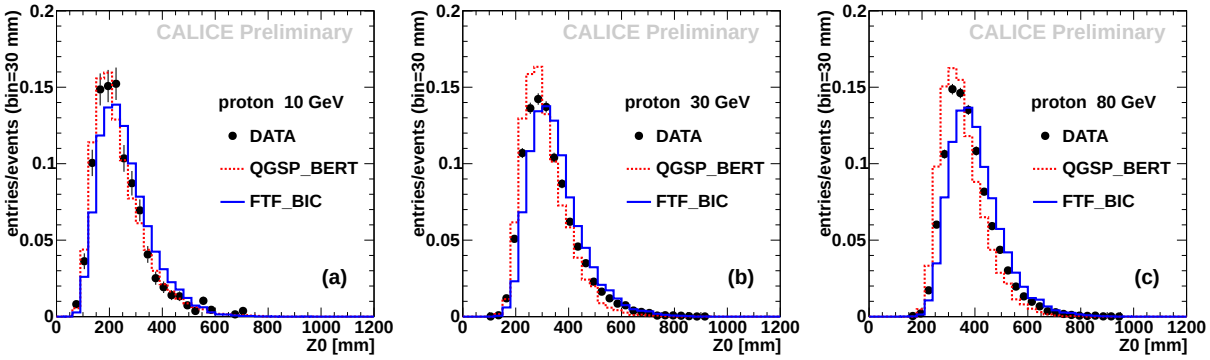

Figure 8: Distributions of the longitudinal centre of gravity for proton-induced showers at initial momentum (a) 10 GeV/c, (b) 30 GeV/c and (c) 80 GeV/c for data (black circles) and QGSP_BERT (red dashed line) and FTF_BIC (blue solid line) physics lists.

deviations within a shower as it is described below. It should be noted that the shower parameters R and $Z0$ extracted from Eq. 1 and 4 respectively correspond to approximately 65% of shower containment. As for 95% of longitudinal (radial) shower containment, it corresponds to $\sim 3 \cdot Z0$ ($\sim 3.3 \cdot R$).

5.1 Mean center of gravity in longitudinal direction

The longitudinal centre of gravity of a hadronic shower in the AHCAL is calculated for each event by means of Eq. 4. This value is estimated w.r.t. shower start to make possible the comparison of different types of hadrons that have different nuclear interaction lengths. The example distributions of the longitudinal centre of gravity $Z0$ for three different energies are presented in Fig. 7 for pions and in Fig. 8 for protons.

The mean longitudinal shower depth $\langle Z0 \rangle$ is extracted from the distributions shown in

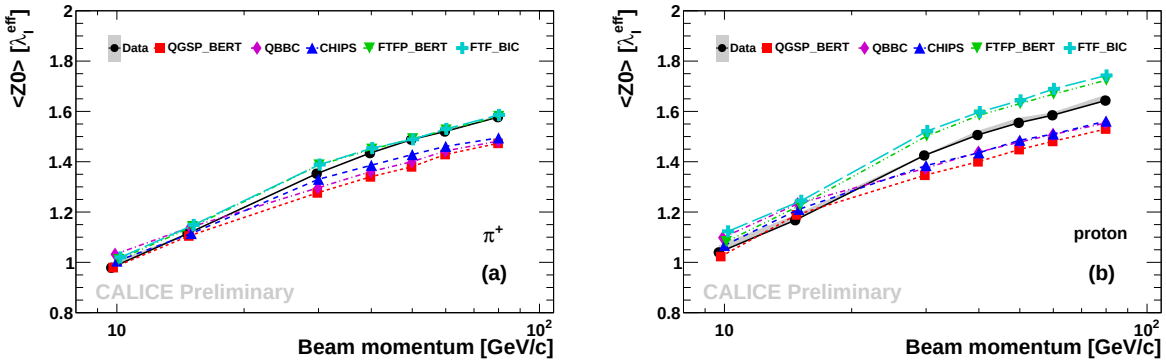

Figure 9: Mean longitudinal centre of gravity of (a) pion and (b) proton-induced showers in units of $\lambda_{\mathrm{I}}^{\mathrm{eff}} = 231$ mm versus beam momentum for data (black circles) and GEANT4 models. Systematic uncertainties for data are shown with grey band.

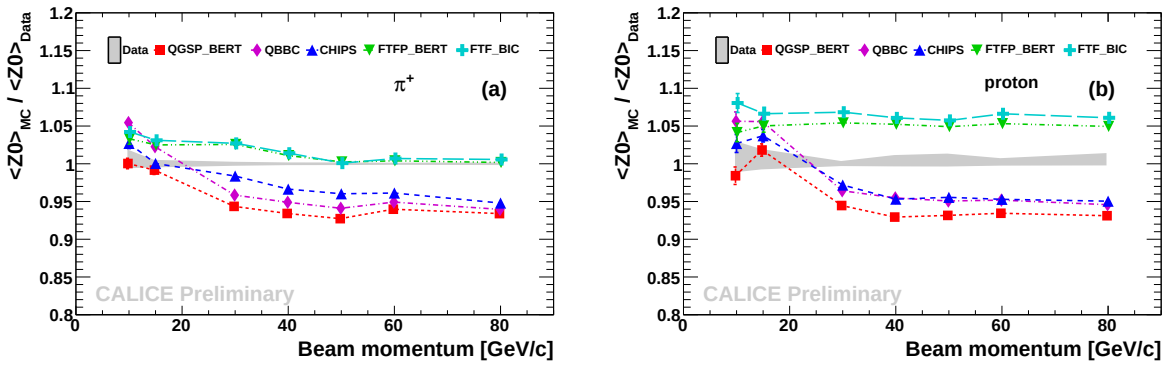

Figure 10: Ratio of mean longitudinal centre of gravity extracted from simulations using different physics lists to that extracted from data versus beam momentum for (a) pion and (b) proton-induced showers. Systematic uncertainties for data are shown with grey band.

Fig. 7 and 8 and increases logarithmically with energy. The corresponding energy dependences of $\langle Z0 \rangle$ are shown in Fig. 9. Fig. 10 shows the ratios of simulations to data. QGSP_BERT physics list gives the best predictions for both pions (Fig. 10a) and protons (Fig. 10b) below 20 GeV. QGSP_BERT, QBBC and CHIPS physics lists underestimate $\langle Z0 \rangle$ by ∼4-8% for both pions and protons above 20 GeV. FTFP_BERT and FTF_BIC physics lists give a very good prediction of $\langle Z0 \rangle$ for pions above 40 GeV and overestimate this value for protons by ∼5%.

The mean values of standard deviation $\langle \sigma_{Z0} \rangle$ estimated using Eq. 5 are of the same order of magnitude as the mean value $\langle Z0 \rangle$ (Fig. 11) and also increase logarithmically with energy. For pions (Fig. 12a), all physics lists except for CHIPS are in coincidence with data below 20 GeV while above 20 GeV the most disagreement (∼5%) shows QGSP_BERT physics list. For protons (Fig. 12b), QBBC and CHIPS are in agreement with data within 2% while QGSP_BERT underestimates and Fritiof-based physics lists overestimate the standard deviation of $Z0$.

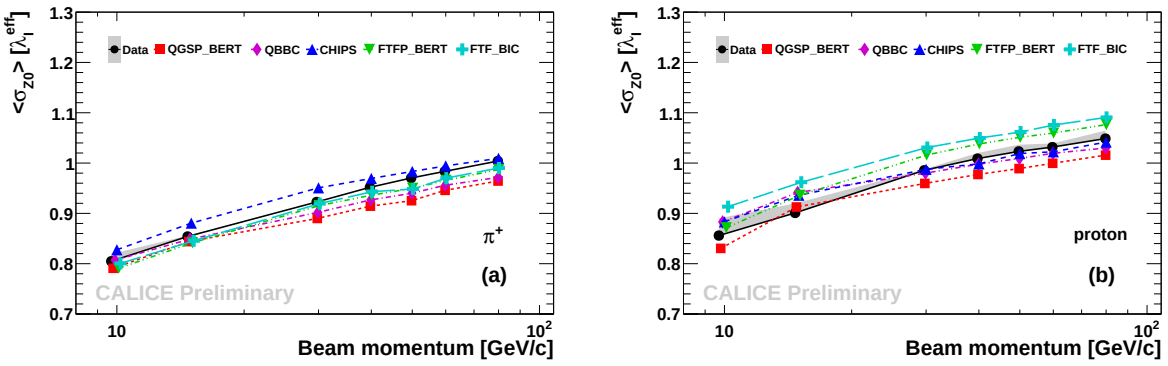

Figure 11: Mean standard deviation of longitudinal centre of gravity of (a) pion and (b) proton-induced showers in units of $\lambda_{\mathrm{I}}^{\mathrm{eff}} = 231$ mm versus beam momentum for data (black circles) and GEANT4 models. Systematic uncertainties for data are shown with grey band.

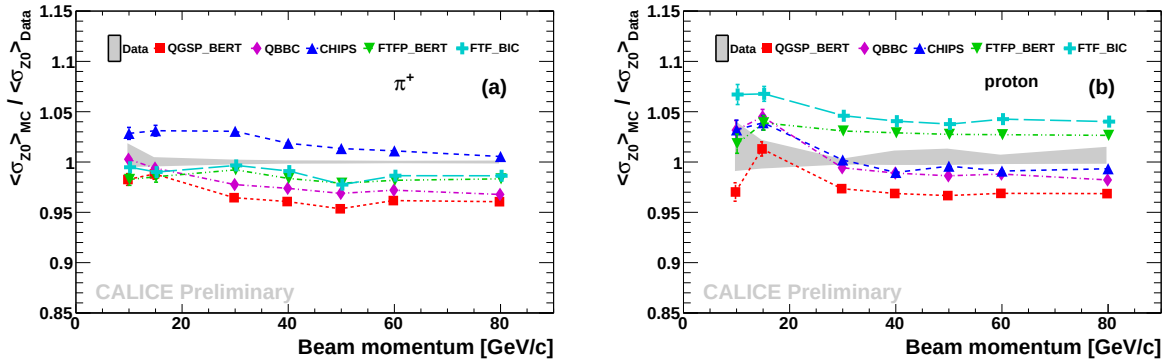

Figure 12: Ratio of mean standard deviation of longitudinal centre of gravity extracted from simulations to that extracted from data versus beam momentum for (a) pion and (b) proton-induced showers. Systematic uncertainties for data are shown with grey band.

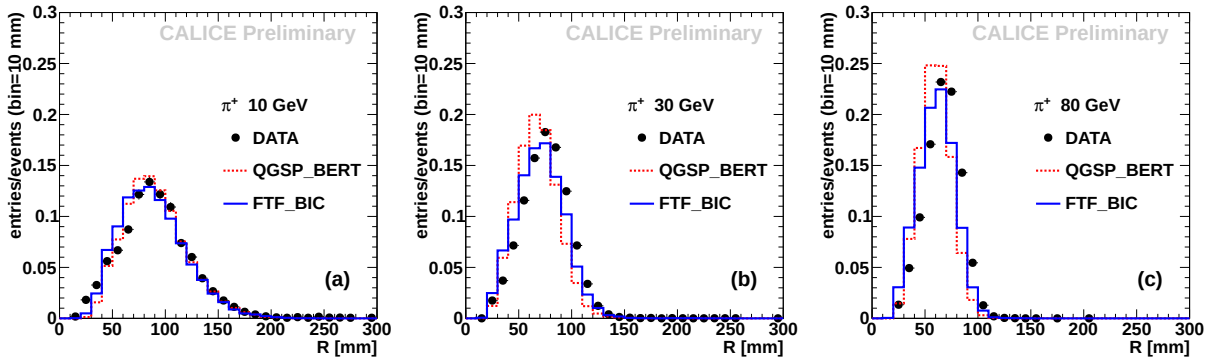

Figure 13: Distributions of the shower radius for pion-induced showers at initial momentum (a) 10 GeV/c, (b) 30 GeV/c and (c) 80 GeV/c for data (black circles) and QGSP_BERT (red dashed line) and FTF_BIC (blue solid line) physics lists.

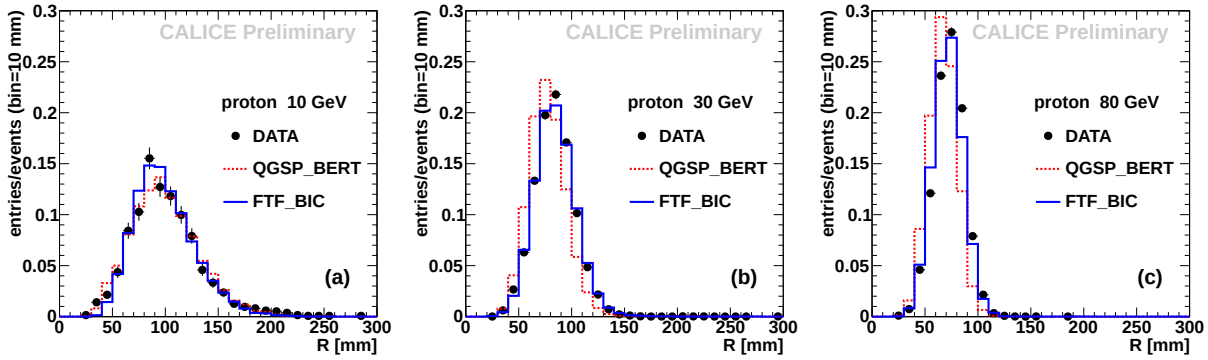

Figure 14: Distributions of the shower radius for proton-induced showers at initial momentum (a) 10 GeV/c, (b) 30 GeV/c and (c) 80 GeV/c for data (black circles) and QGSP_BERT (red dashed line) and FTF_BIC (blue solid line) physics lists.

5.2 Mean shower width

The distributions of the shower radius estimated using Eq. 1 are presented in Fig. 13 for pions and in Fig. 14 for protons. From these distributions the mean value $\langle R \rangle$ is extracted.

The energy dependences of mean shower radius are shown in Fig. 15. The values of $\langle R \rangle$ decrease logarithmically with increasing energy and this behaviour is well reproduced by all studied physics lists. The pion (proton) showers are observed to be narrower by ∼25% (∼30%) at 80 GeV than at 10 GeV. This is explained by the increase of electromagnetic fraction in hadronic shower, since electromagnetic sub-showers tend to be much more compact. The ratio of simulations to data is shown in Fig. 16a. The best prediction of shower radius for pions is given by the CHIPS physics list while other physics lists underestimate $\langle R \rangle$ by ∼10%. For protons (Fig. 16b), all physics lists, except for CHIPS, coincide with data within uncertainties at 10 GeV and the best prediction in the studied energy range is given by FTF_BIC physics list (within ∼2%). The underestimation of

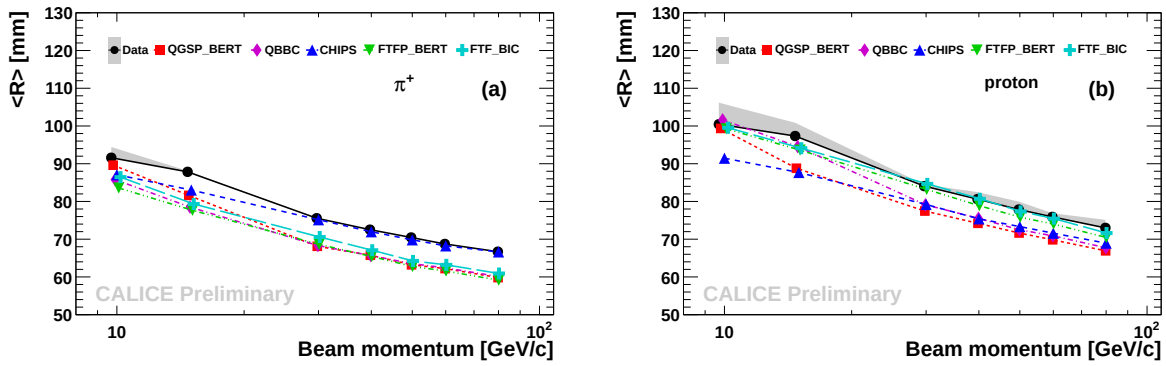

Figure 15: Mean radial width of (a) pion and (b) proton-induced showers versus beam momentum for data (black circles) and GEANT4 models. Systematic uncertainties for data are shown with grey band.

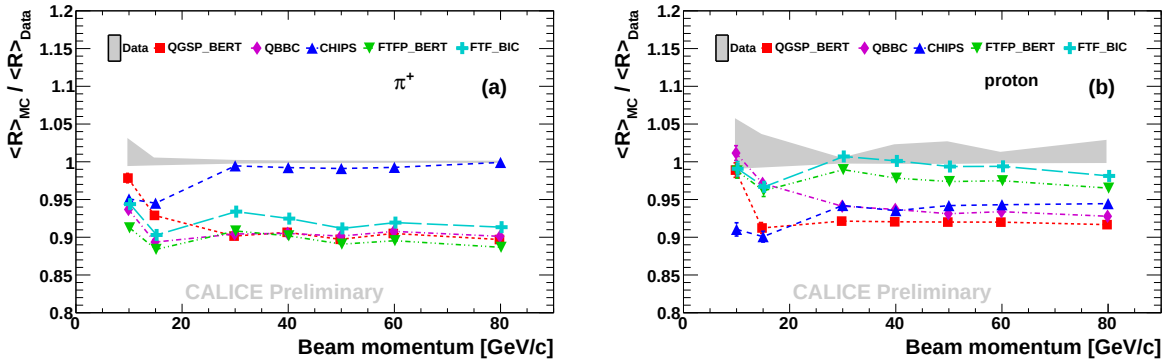

Figure 16: Ratio of mean radial width extracted from simulations to that extracted from data versus beam momentum for (a) pion and (b) proton-induced showers. Systematic uncertainties for data are shown with grey band.

mean shower radius for protons above 20 GeV by QBBC, CHIPS and QGSP_BERT physics lists is ∼8-10%.

The mean standard deviations $\langle\sigma_R\rangle$ are of the same order of magnitude as the mean values $\langle R\rangle$ as follows from Fig. 17 but decrease more slowly with energy. For pions (Fig. 18a), all physics lists underestimate σ_R in all studied energy range. The best prediction is again given by CHIPS (within ∼2% from data) and the higher disagreement is shown by FTFP_BERT (up to ∼6%). For protons (Fig. 12b), the FTF_BIC physics list gives a very good prediction in all studied energy range while greatest underestimation of $\langle\sigma_R\rangle$ is observed for CHIPS (∼6%).

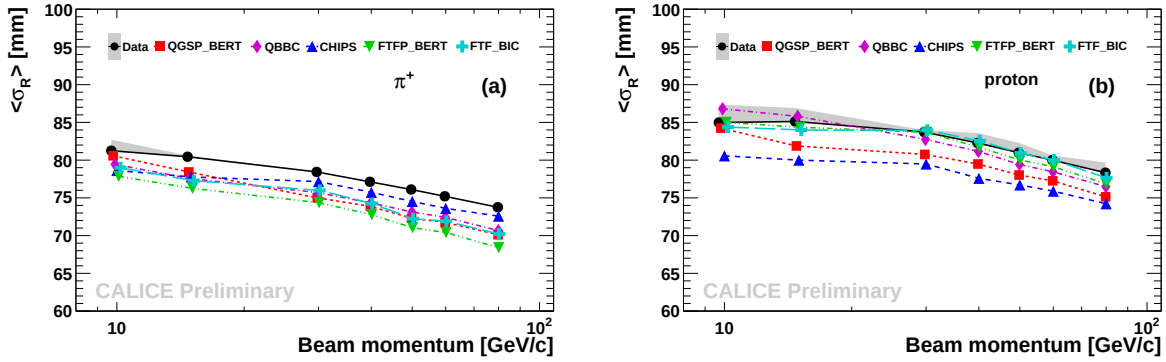

Figure 17: Mean standard deviation of radial width of (a) pion and (b) proton-induced showers versus beam momentum for data (black circles) and GEANT4 models. Systematic uncertainties for data are shown with grey band.

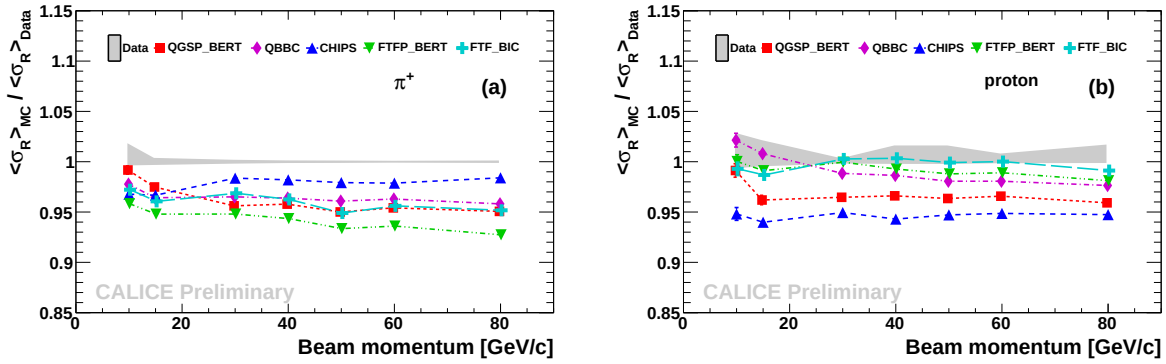

Figure 18: Ratio of mean standard deviation of radial width extracted from simulations to that extracted from data versus beam momentum for (a) pion and (b) proton-induced showers. Systematic uncertainties for data are shown with grey band.

6 Conclusion

In this study, global parameters of hadronic showers induced by positive hadrons in the CALICE analogue scintillator-steel hadronic calorimeter were analysed: calorimeter response and resolution, longitudinal centre of gravity and shower radius. Data were collected during CALICE test beam campaigns at CERN in 2007 and at FNAL in 2009 and cover the range of initial particle momentum from 10 to 80 GeV/c. The offline event selection procedure was implemented including pion from proton separation using stored signal from a threshold Čerenkov counter. Simulation was performed with five physics lists from GEANT4 version 9.4: QGSP_BERT, QBBC, CHIPS, FTFP_BERT and FTF_BIC.

Using shower start finding algorithm, the nuclear interaction length in the CALICE AHCAL for pions and protons was estimated and was observed to be in agreement between data and simulations and in good agreement with PDG data for both pions and protons.

The calorimeter response for positive pions in test beam data is linear in the studied energy range within ±2%. The deficiency of calorimeter response for protons comparing to that for pions which cannot be explained by the difference in available energy is ∼2-4%. All studied GEANT4 physics lists predict non-linear behaviour of pion response. The best agreement with data (within ±4% in studied energy range for pions and ±1% for protons above 20 GeV) is provided by the FTF_BIC physics list. The predictions of CHIPS physics list are in very good agreement with data for both pions and protons below 20 GeV.

For test beam data, the fractional energy resolution for protons is in agreement with that for pions within uncertainties. The best prediction of fractional resolution for both pions and protons can be obtained with QGSP_BERT physics list in the analysed energy range. Fritiof-based physics lists overestimate the fractional resolution above 50 GeV, while QBBC and CHIPS underestimate it below 20 GeV.

One of the global observables that characterises a spatial development of hadronic shower is the mean shower depth. It is defined as the longitudinal centre of gravity w.r.t. shower start and on average accounts for ∼65% of longitudinal shower containment in the calorimeter. The longitudinal shower depth increases logarithmically with energy and is ∼5% lower for pions than for protons. The mean standard deviations of the shower depth are of the same order of magnitude as the mean depth value. For both pions and protons, QGSP_BERT, QBBC and CHIPS give good predictions below 20 GeV and underestimate the mean shower depth by ∼5% above 20 GeV. FTFP_BERT and FTF_BIC physics lists are in very good agreement with data above 30 GeV for pions and overestimate mean shower depth for protons by ∼5%.

Another global observable that describes radial shower development is the mean shower radius. It is calculated as a weighted sum of radial distances from hits to shower axis and accounts for ∼65% of radial shower containment in the calorimeter. The mean shower radius decreases logarithmically with increasing energy and is ∼10% lower for pions than for protons. Most physics lists underestimate the mean shower radius for both pions and protons by ∼6-10%, except for CHIPS that is in good agreement with pion data above

20 GeV and FTF_BIC physics list that predicts mean shower radius for protons with ∼2% accuracy.

7 Acknowledgements

The author would like to thank Lars Weuste and Alex Kaplan for providing the simulated samples. The author is also very grateful to Vasiliy Morgunov, Oleg Markin, Eugeny Tarkovsky, Sergey Morozov, Angela-Isabela Lucaci-Timoce and Nils Feege for many fruitful discussions.

References

[1] R. Wigmans, *Calorimetry: Energy Measurement in Particle Physics*, International Series of Monographs on Physics, vol. 107, Oxford University Press, Oxford, 2000.

[2] D. E. Groom, *Energy flow in a hadronic cascade: Application to hadron calorimetry*, Nucl. Instrum. Meth. **A572** (2007) 633-653.

[3] H. Abramowicz *et al.*, *The response and resolution of an iron-scintillator calorimeter for hadronic and electromagnetic showers between 10 GeV and 140 GeV*, Nucl. Instrum. Meth. **180** (1981) 429-439.

[4] D. Acosta *et al.*, *Electron, pion and multiparticle detection with a lead/scintillating-fiber calorimeter*, Nucl. Instrum. Meth. **A308** (1991) 481-508.

[5] P. de Barbaro (For the CDF Plug Upgrade Group), *Test Beam Performance of the CDF Plug Upgrade Hadron Calorimeter*, FERMILAB-Conf-98/057-E.

[6] T. A. Gabriel, D. E. Groom, P. K. Job, N.V. Mokhov and G. R. Stevenson, *Energy dependence of hadronic activity*, Nucl. Instrum. Meth. **A338** (1994) 336-347.

[7] N. Akchurin, *On the differences between high-energy proton and pion showers and their signals in a non-compensating calorimeter*, Nucl. Instrum. Meth. **A408** (1998) 380396.

[8] P. Adragna, *Measurement of pion and proton response and longitudinal shower profiles up to 20 nuclear interaction lengths with the ATLAS Tile calorimeter*, Nucl. Instrum. Meth. **A615** (2010) 158181.

[9] C. Adloff *et al.* [CALICE collaboration] *Hadronic energy resolution of a highly granular scintillator-steel calorimeter using software compensation techniques*, 2012 JINST **7** P09017.

[10] C. Adloff *et al.* [CALICE collaboration], *Design and electronics commissioning of the physics prototype of a Si-W electromagnetic calorimeter for the International Linear Collider*, 2008 JINST **3** P08001.

[11] C. Adloff *et al.* [CALICE collaboration], *Construction and commissioning of the CALICE analog hadron calorimeter prototype*, 2010 JINST **5** P05004.

[12] C. Adloff *et al.* [CALICE collaboration], *Construction and performance of a silicon photomultiplier/extruded scintillator tail-catcher and muon-tracker*, 2012 JINST **7** P04015.

[13] N. Feege, *Low-energetic hadron interactions in a highly granular calorimeter*, DESY-THESIS-2011-048.

[14] C. Adloff *et al.* [CALICE collaboration], *Electromagnetic response of a highly granular hadronic calorimeter*, 2011 JINST **6** P04003.

[15] K. Seidel, *Si-W-Ecal treatment for HCAL only analysis and development of event selection processors*, Talk on AHCAL Main Meeting, DESY, 20.01.2011. http://ilcagenda.linearcollider.org/conferenceDisplay.py?confId=4932

[16] The CALICE Collaboration, *Local and global software compensation approaches: application to test beam data*, CALICE Analysis Note CAN-035 (2011).

[17] The CALICE Collaboration, *Pion Showers in the CALICE AHCAL Prototype*, CALICE Analysis Note CAN-026 (2011).

[18] S. Agostinelli *et al.* [GEANT4 Collaboration], *Geant4: A Simulation toolkit*, Nucl. Instrum. Meth. **A506** (2003) 250.

[19] J. Beringer *et al.* (Particle Data Group) *The Review of Particle Physics*, Phys. Rev. **D86**, 010001 (2012).

[20] A. Lucaci, *HCAL prototype in the test beam Mokka model*, https://twiki.cern.ch/twiki/bin/view/CALICE/SoftwareMain/hcalTBeam.pdf.

A Positron selection for FNAL runs

The electromagnetic showers are known to be more compact than hadronic ones. The compactness of a shower in a given event can be characterised by the shower radius R (from Eq. 1) and longitudinal centre of gravity Z (from Eq. 2). The examples of joint distributions of R and Z for pions and positrons are shown in Fig. 19. Showers with $R < 37$ mm and $Z < 260$ mm are considered to be initiated by positrons. The black rectangle corresponding to this cut is shown in all plots of Fig. 19. The estimated efficiencies of positron identification with such a procedure are indicated in Section 2.2.

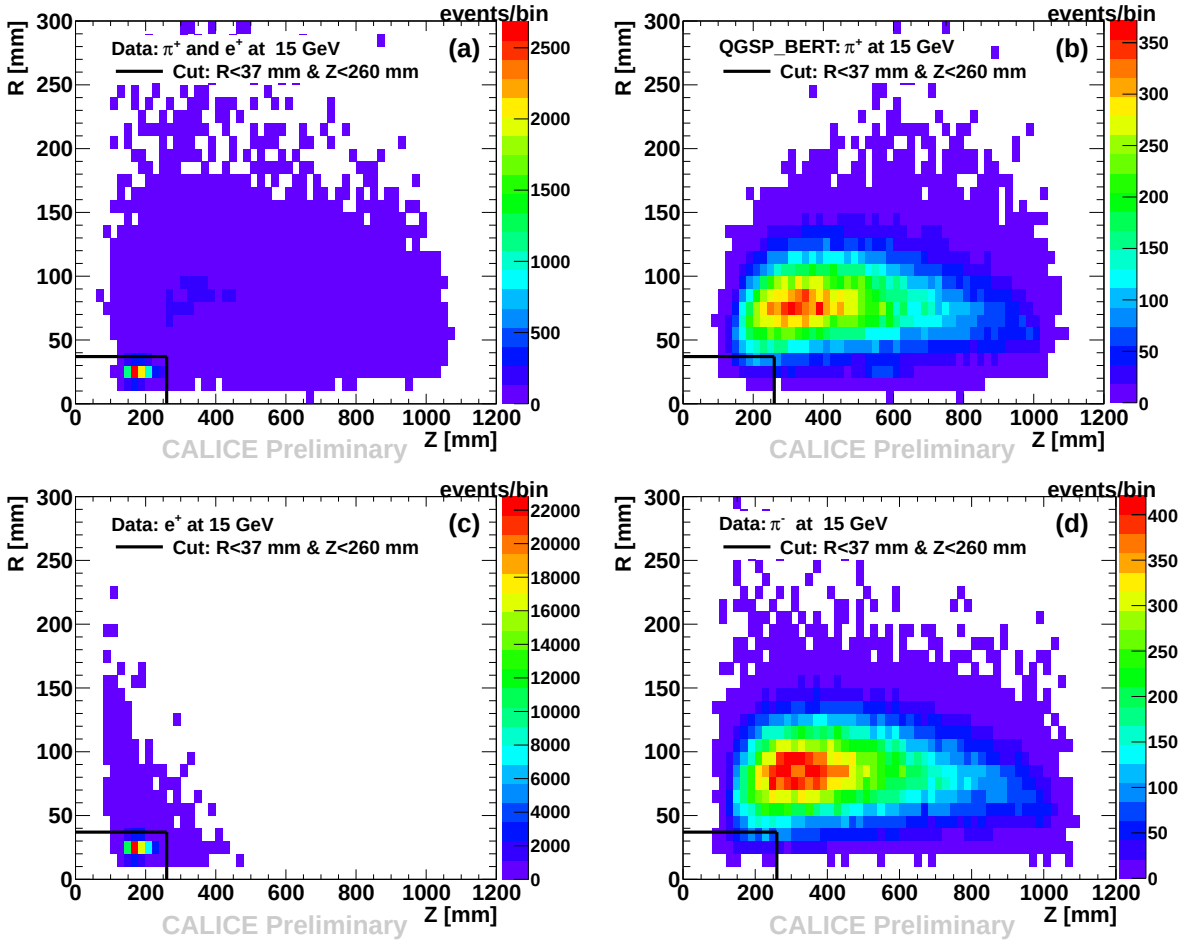

Figure 19: Joint distributions of shower radius R and longitudinal centre of gravity Z for particles with initial energy 15 GeV: (a) mixed data sample of pions and positrons, (b) simulated sample of pions, (c) data sample of positrons and (d) data sample of negative pions. The samples (a), (b) and (c) correspond to the setup without ECAL, while sample (d) is from run taken with complete setup and contains selected events with track in ECAL. The black rectangle shows the cut applied to reject positrons.

B Estimation of systematic uncertainties

Let us suppose there is a selection procedure applied to our sample to remove contaminating admixture. The efficiency of our selection procedure is characterised by two values: the probability ϵ of correct identification of contaminating admixture and the probability τ of correct identification of our events of interest. After selection procedure the number of selected events is N_{selected} and the number of rejected events is N_{rejected}. The value of given observable calculated as a mean for selected sample M_{measured} might be shifted if the mean for admixture $M_{\text{admixture}}$ differs from the true mean of the pure sample of interest M_{true}. The following general expression can be derived to estimate a relative bias δ_{sys} due to contamination:

$$\delta_{\text{sys}} = \frac{M_{\text{measured}} - M_{\text{true}}}{M_{\text{measured}}} = \frac{(1-\tau(\mu+1))(1-\epsilon)(1-\Delta)}{\epsilon\tau - \mu\tau(1-\epsilon)}, \tag{11}$$

where $\mu = \frac{N_{\text{rejected}}}{N_{\text{selected}}}$ and Δ is the ratio of the mean calculated for pure contaminating admixture to the observed mean of selected sample. The uncertainty δ_{sys} is very sensitive to the efficiencies of admixture identification ϵ. The low values ϵ (below 0.9) can result in singularities even at reasonable values of μ. The efficiencies ϵ achieved in this particular study are higher than 0.9 and μ does not exceed 6. In this case the sign of δ_{sys} depends on whether the ratio Δ is greater or less than 1.

Positron admixture. The values of ϵ and τ for Eq. 11 were obtained from the efficiencies of positron identification and the fraction of misidentified hadrons respectively (see Section 2.2). The value of μ is estimated for the corresponding subsamples after event selection. The mean reconstructed energy, mean shower depth and mean shower radius for positron samples were estimated from positron runs to calculate the corresponding values of Δ. The systematic uncertainties due to positron admixture δ_{e^+} calculated using Eq. 11 for studied observables are shown in Tables 4, 5 and 6. Due to positron admixture the mean reconstructed energy is overestimated while mean shower depth and width are underestimated.

Pion admixture in proton samples. The pion from proton separation in the test beam experiments fully relies on the Čerenkov counter efficiency. As the pressure in gaseous Čerenkov detector used was set well below the proton threshold, we assume here that the misidentification of protons is negligible (that corresponds to $\tau = 1$ in Eq. 11). To estimate the efficiency of Čerenkov counter, the procedure of muon identification is used which is based on the calorimeter data only and is itself independent on the Čerenkov efficiency. Assuming that the efficiency for pions ϵ_{pion} is approximately the same as for muons ϵ_{muon} the value of $\epsilon = \epsilon_{\text{pion}}$ for Eq. 11 can be calculated as follows:

$$\epsilon = \epsilon_{\text{pion}} \approx \epsilon_{\text{muon}} = \frac{N_{\text{muon}}^{\text{cher}}}{N_{\text{muon}}^{\text{total}}}, \tag{12}$$

where $N_{\text{muon}}^{\text{cher}}$ is the number of identified muons that gave signal in the Čerenkov detector, $N_{\text{muon}}^{\text{total}}$ is the total number of muons identified using the independent procedure. The systematic uncertainty δ_η is asymmetric and is shown in Tables 4, 5 and 6. The admixture of pions in proton samples results in overestimation of reconstructed energy and underestimation of shower longitudinal and radial sizes. The relative systematic uncertainties of $\langle\sigma_{Z0}\rangle$ are almost the same as of $\langle Z0\rangle$. The relative systematic uncertainties of $\langle\sigma_R\rangle$ are approximately twice lower than those of $\langle R\rangle$

To estimate the nuclear interaction length for protons using Eq. 8, the purity values are required. The purity of proton sample η, i.e. the ratio of the number of real protons to the number of identified protons, can be estimated as follows:

Table 4: Systematic uncertainties for reconstructed energy E_{reco}.

Beam momentum, GeV/c	Pion				Proton				
	δ_{MIP} %	δ_{e^+} %	total		δ_{MIP} %	δ_{e^+} %	δ_{η} %	total	
			down,%	up,%				down,%	up,%
10	0.9	+0.8	1.20	0.9	0.9	+0.1	+6.6	6.7	0.9
15	0.9	+0.1	0.91	0.9	0.9	+0.1	+2.9	3.0	0.9
30	0.9	0	0.90	0.9	0.9	0	+0.3	0.95	0.9
40	0.9	0	0.90	0.9	0.9	0	+1.2	1.5	0.9
50	0.9	0	0.90	0.9	0.9	0	+1.2	1.5	0.9
60	0.9	0	0.90	0.9	0.9	0	+0.5	1.0	0.9
80	0.9	0	0.90	0.9	0.9	0	+0.8	1.2	0.9

Table 5: Systematic uncertainties for mean longitudinal centre of gravity $\langle Z0 \rangle$.

Beam momentum, GeV/c	Pion				Proton			
	δ_{e^+} %	total		δ_{e^+} %	δ_{η} %	total	
		down,%	up,%			down,%	up,%
10	-1.5	0	1.5	-0.2	-2.8	0	2.8
15	-0.2	0	0.2	-0.1	-1.8	0	1.8
30	0	0	0	0	-0.2	0	0.2
40	0	0	0	0	-1.1	0	1.1
50	0	0	0	0	-1.3	0	1.3
60	0	0	0	0	-0.7	0	0.7
80	0	0	0	0	-1.4	0	1.4

$$\eta = 1 - \frac{N_\pi}{N_{\mathrm{p}}} \frac{1 - \epsilon_{\mathrm{pion}}}{\epsilon_{\mathrm{pion}}}, \tag{13}$$

where N_π (N_{p}) is the number of pions (protons) identified using Čerenkov counter. The corresponding values of Čerenkov counter efficiency and purity of analysed proton samples are shown in Table 3 (Section 2.4). The errors of ϵ_{muon} are estimated basing on the available statistics of muon events and are propagated to the uncertainties of purities.

C Calorimeter response and resolution for QBBC, CHIPS and FTFP_BERT physics lists

The linearity of the CALICE Sc-Fe AHCAL for data as well as QBBC, CHIPS and FTFP_BERT physics lists is shown in Fig. 20, 21, 22. The comparison of fractional energy

Table 6: Systematic uncertainties for mean shower radius $\langle R \rangle$.

Beam momentum, GeV/c	Pion			Proton			
	δ_{e^+}	total		δ_{e^+}	δ_η	total	
	%	down,%	up,%	%	%	down,%	up,%
10	-2.7	0	2.7	-0.4	-5.7	0	5.7
15	-0.4	0	0.4	-0.1	-3.6	0	3.6
30	0	0	0	0	-0.5	0	0.5
40	0	0	0	0	-2.3	0	2.3
50	0	0	0	0	-2.7	0	2.7
60	0	0	0	0	-1.3	0	1.3
80	0	0	0	0	-2.9	0	2.9

resolutions is presented in Fig. 23.

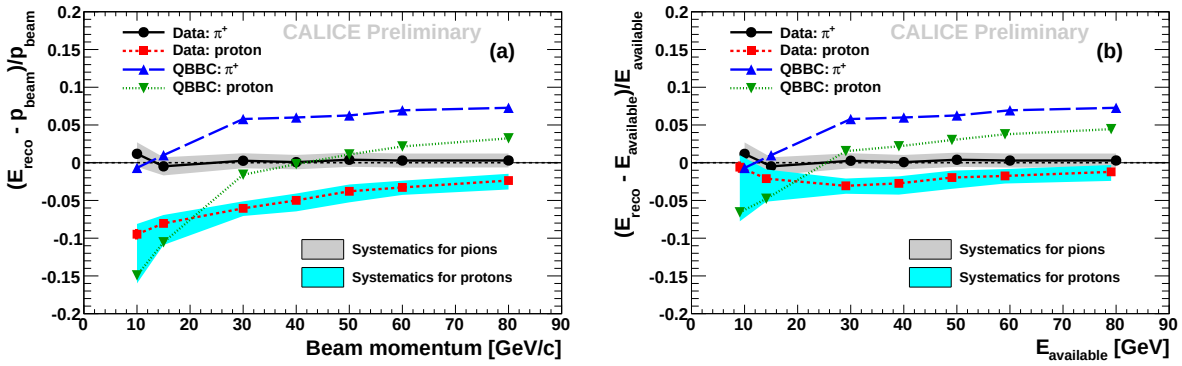

Figure 20: Relative residuals of reconstructed energy E_{reco} to (a) beam momentum and (b) available energy for data (black circles for pions and red squares for protons) and QBBC physics list (blue triangles for pions and green down triangles for protons). Systematic uncertainties for data are shown with grey band for pions and cyan band for protons.

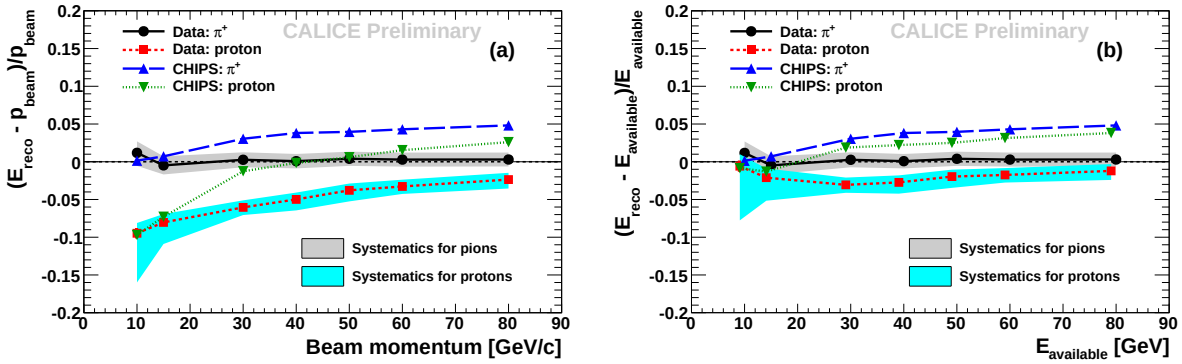

Figure 21: Relative residuals of reconstructed energy E_{reco} to (a) beam momentum and (b) available energy for data (black circles for pions and red squares for protons) and CHIPS physics list (blue triangles for pions and green down triangles for protons). Systematic uncertainties for data are shown with grey band for pions and cyan band for protons.

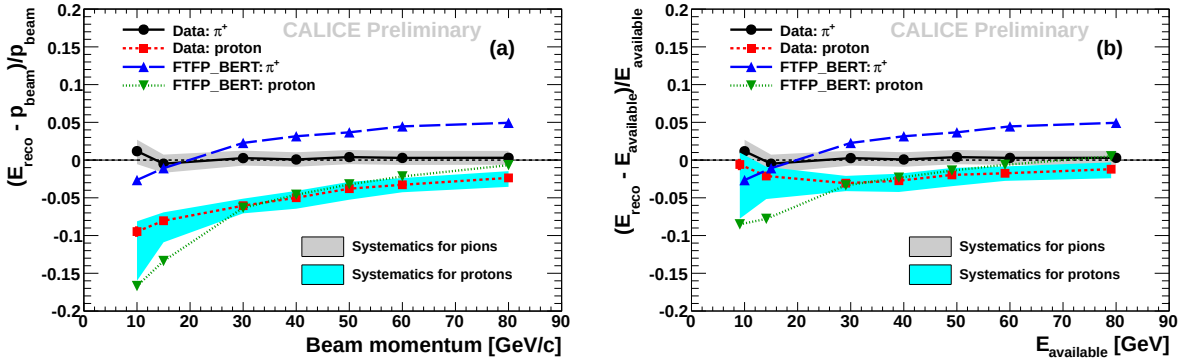

Figure 22: Relative residuals of reconstructed energy E_{reco} to (a) beam momentum and (b) available energy for data (black circles for pions and red squares for protons) and FTFP_BERT physics list (blue triangles for pions and green down triangles for protons). Systematic uncertainties for data are shown with grey band for pions and cyan band for protons.

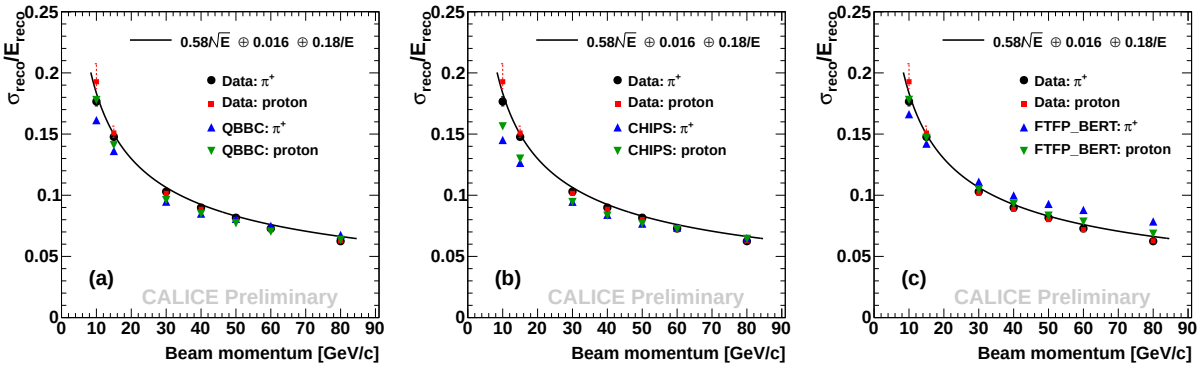

Figure 23: Fractional resolution versus beam momentum for data (black circles for pions and red squares for protons) and simulations (blue triangles for pions and green down triangles for protons) for (a) QBBC, (b) CHIPS and (c) FTFP_BERT physics lists.